Imaging Bone Water Compartments

Jiang Du
Department of Radiology
University of California, San Diego
San Diego, California

Background

Osteoporosis (OP) is a metabolic bone disease, which affects more than 10 million people in the USA and leads to over 2 million fractures every year – more than heart attacks, strokes and breast cancer combined [1-5]. In addition, OP results in serious long-term disability and death in a large number of patients. About 80% of the skeleton is cortical bone, and about 80% of all fractures in old age arise at sites that are mainly cortical [6]. It is of critical importance to 'understand' cortical bone structure and to develop techniques to evaluate bone compartments so as to evaluate bone quality non-invasively.

Cortical bone is a composite material consisting of mineral (~43% by volume), organic matrix (~35%) and water (~22%) [7]. Bone mineral provides stiffness and strength, while collagen provides ductibility and the ability to absorb energy before fracturing. Bone water contributes to viscoelasticity and poroelasticity [8]. Although bone is a simple composite of these three components, its structure is highly complex and hierarchical [9], as shown in **Figure 1**. The material composition and structural design determines the unique strength of bone.

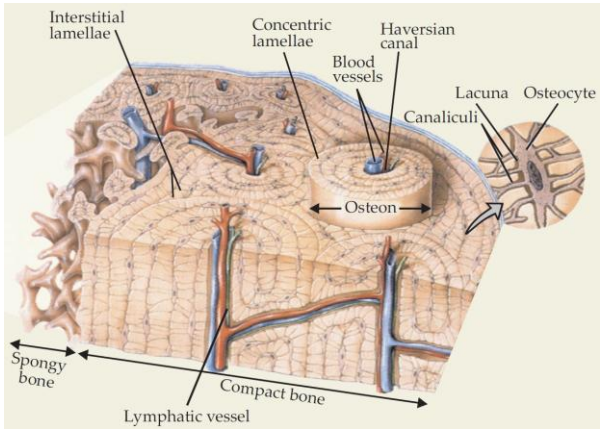

Fig 1 Macroscopic bone structure from Ref 9.

Imaging of bone has been of central importance since Roentgen produced the first radiograph in 1895. Dual-energy X-ray absorptiometry (DEXA) and computed tomography (CT) have been used for quantitative analysis including the measurement of bone mineral density (BMD). The organic matrix and water, which together represent ~57% of bone by volume, are not accessible with these techniques [10-22]. BMD alone predicts fractures with only a 30-50% success rate [23-39]. Overall fracture risk increases 13-fold from ages 60 to 80, but it is estimated that the decrease in BMD alone would only explain a doubling of this fracture risk [11]. The missing factor may be the contribution of bone organic matrix and water. Water in cortical bone occurs at various locations and in different states [7]. A small fraction of this water exists in 'free' form in Haversian canals (typical diameters > 30 μm) as well as lacunae (~10 μm) and canaliculi (~0.5 μm). A larger portion of cortical bone water exists in 'bound' form, either tightly bound to the crystals of the apatite-like mineral or loosely bound to the organic matrix [40-50]. Bound water concentration provides an indirect measure of organic matrix density [45-47]. Free water concentration can potentially provide a surrogate measure of cortical porosity [48-50]. However, neither DEXA nor CT is able to detect bound and free bone water.

A recent study shows that bound and free water make different contributions to the mechanical properties of bone [41], making it important to separate the two in studies of bone quality. However, distinguishing free water from water bound to the organic matrix and water bound to the mineral is a challenge. Recently nuclear magnetic resonance (NMR) spectroscopy has been used for this purpose [41-43]. In these studies multi-component analysis of the Carr-Purcell-Meiboon-Gill (CPMG) spin echo and free induction decay (FID) data was used to provide a T2/T2* spectra which reflected bound (short T2/T2*) and free water (longer T2/T2*) components [41-43]. Water that was very tightly bound to mineral was not detectable with these techniques. Furthermore, these prior techniques are only applicable to in vitro samples due to the requirement of high performance NMR spectrometers and small sample sizes.

In magnetic resonance imaging (MRI) cortical bone is typically regarded as 'invisible' when it is studied with conventional clinical pulse sequences [51]. However, free water in cortical bone has a short T2* but a relatively long T2 [41-44], and conventional fast spin echo (FSE) sequences can in principle have TEs short enough to image this portion of water. In recent years, ultrashort echo time (UTE) MRI sequences with nominal TEs of less than 100 μs have been developed to image cortical bone [45-60]. These sequences can potentially detect free water and water bound to the organic matrix [45-47]. In this lecture I will first introduce techniques for morphological imaging of bone water compartments (total, bound and free water) followed by quantitative imaging of these bone water compartments using clinical whole-body MR scanners.

Morphological Imaging of Bone Water Compartments

As mentioned above, free water in cortical bone can potentially be imaged by conventional clinical FSE sequences, but remains 'invisible' to conventional clinical gradient recalled echo (GRE) sequences due to its long T2 but short T2*. Two-dimensional (2D) and 3D UTE sequences can potentially image both bound and free water, while adiabatic inversion recovery prepared UTE (IR-UTE) sequences can potentially image water bound to the organic matrix using clinical MR scanners. Each of these techniques will be discussed in the following sections.

FSE Imaging of Free Water in Cortical Bone

Recent NMR spectroscopy studies have demonstrated that free water in bone pores can have T2 values of 100 ms or longer [40-44]. This portion of bone water can be detected with conventional clinical FSE sequences with TEs of around 15 ms [59]. **Figure 2** shows a representative axial slice of a bone sample imaged with the conventional clinical 2D FSE sequence with a voxel size of 78×78×500 μm^3 and a SNR of 19.5 ± 3.7. Cortical bone structure is well depicted, especially in the zoomed region shown in Figure 2B. The high signals are likely to be from free water residing in the Haversian system which has relatively long T2.

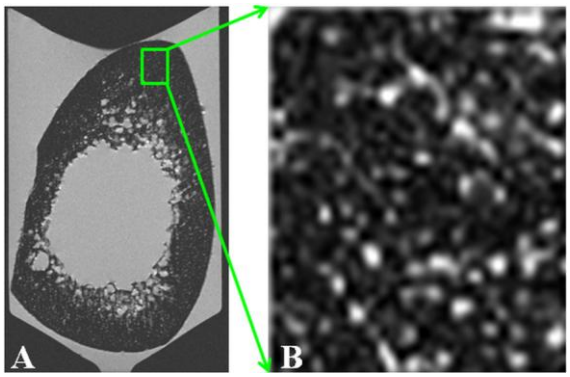

Fig 2 Axial 2D FSE imaging of a bone sample immersed in saline (A) and a zoom of a sub-region (B). Fine structure corresponding to free water residing in the Haversian system of bone is seen.

Figure 3 shows representative axial and sagittal slices of another bone sample imaged with 2D FSE (SNR = 23.1 ± 7.4) and GRE (SNR = 3.2 ± 1.9) sequences as well as with μCT. The high

signal shown on the FSE image correlates with the signal void seen on the μCT images. No signal was observed with the clinical 2D GRE sequence.

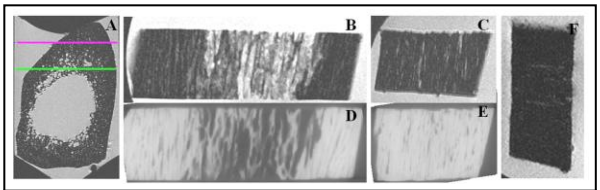

Fig 3 Axial (A) and two representative sagittal 2D FSE images of a bone sample immersed in saline, corresponding to the green line (B) and red line (C), respectively, and the corresponding μCT images (D, E), as well as a representative sagittal 2D GRE image (F). The high signal in (B) and (C) corresponds with the dark signal in (D) and (E), consistent with the presence of long T2 water components in the Haversian system. The 2D GRE sequence shows little signal from cortical bone (F).

This long T2 bone water component has only recently been demonstrated with clinical SE sequences on whole body scanners [59]. There are three technical challenges for directly imaging bone porosity with MRI. Firstly, cortical bone has a very low free water concentration which makes it difficult to image with proton based MR techniques. The majority of bone water exists in the form of bound water (bound to the organic matrix or mineral). Only a small fraction (~20%) of the total water exists in free form in the Haversian and Lacunocanalicular systems. Water typically occupies less than 30% of bone by volume and free water occupies less than 6% of bone by volume. Secondly, there is a lack of dynamic range in direct imaging of bone water. Cortical bone is surrounded by bone marrow (inside) and muscle (outside). Both of these tissues have far higher mean proton densities (80-90% by volume). Thirdly, there is a need for high spatial resolution and thus associated low SNR in imaging bone architecture. Free water resides in the fine structures of cortical bone, and requires a spatial resolution of less than 100 μm for its depiction. The true resolution of MR sequences is reduced due to the short T2* of both the free and bound water components [7]. A small coil in close proximity to bone is required for optimal imaging. Given the longitudinal structure of Haversian canals, axial imaging with thick slices is one way to improve SNR for clinical assessment of cortical bone structure. Another way is to focus on "giant" canals with diameters of 300 μm or larger. Studies by Bell et al have shown that "giant" canals with diameters > 385 μm make a substantial contribution to cortical porosity, and have a markedly negative influence on the ability of cortical bone to withstand the stresses associated with a fall [61]. Therefore, direct imaging of "giant" canals with 2D FSE axial imaging, thick slices and high performance localized coils may make it possible to evaluate free water, and hence porosity using clinical MR scanners.

UTE Imaging of Bound and Free Bone Water

The existence of two distinct components in cortical bone was demonstrated in **Figure 4**, which shows selected UTE images of a cortical bone sample with progressively increasing TEs ranging from 8 μs to 12 ms as well as the single and bi-component curve fitting of UTE T2* signal decay. A SNR (~54) and in-plane spatial resolution (0.3×0.3 mm^2) was achieved in under 2 minutes scan time. Single component fitting of the UTE T2* decay curve from an ROI drawn in cortical bone shows a short T2* of 0.66 ± 0.05 ms. However, there is systematic residual signal with errors greater than 10% around TEs of 2 to 4 ms, suggesting the existence of another water component with a longer T2*. Excellent fitting was achieved with the bi-component model, which demonstrated two distinct components one with a short T2* of 0.34 ms and the other with a long T2* of 2.92 ms. The shorter T2* component accounts for 75.4% of the total UTE MR signal decay, and the longer T2* component accounts for the other 24.6% of the signal decay. The residual signal was reduced to less than 2%, demonstrating that the bi-component model accounts well for the UTE T2* decay behavior.

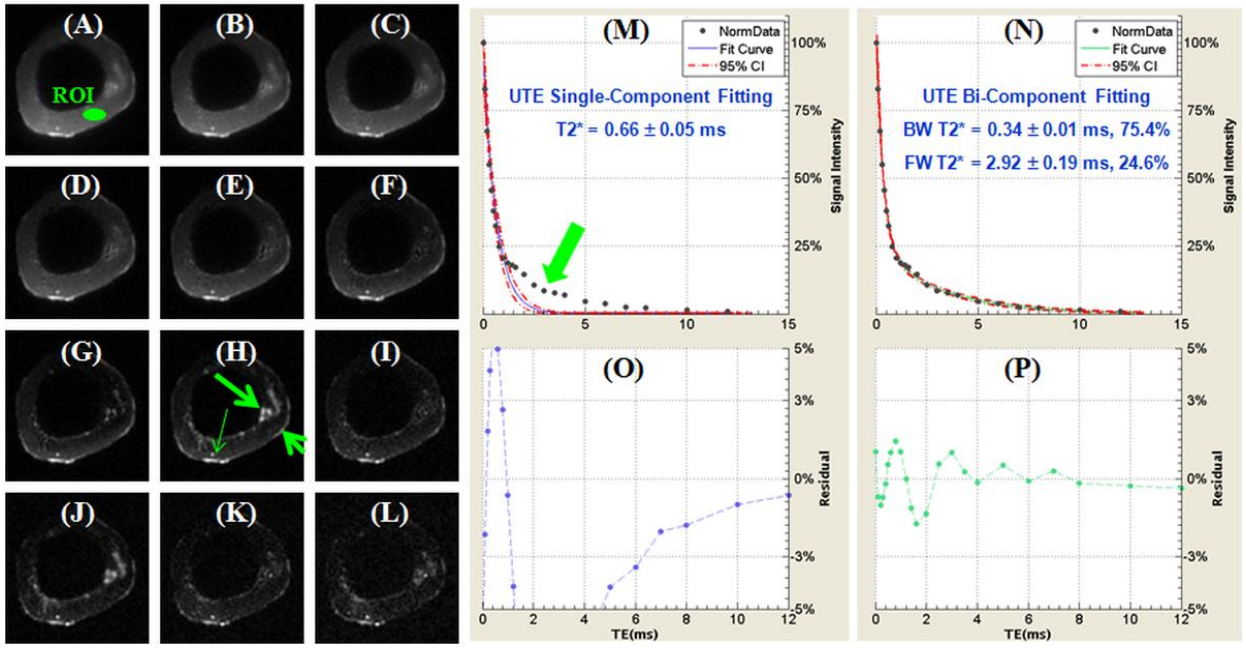

Fig 4 Selected non-slice selective 2D UTE imaging of a human cortical bone sample immersed in PFOB with TEs of 8 μs (A), 0.2 ms (B), 0.4 ms (C), 0.6 ms (D), 0.8 ms (E), 1.2 ms (F), 1.6 ms (G), 2.0 ms (H), 3.0 ms (I), 4.0 ms (J), 5.0 ms (K), and 6.0 ms (L), as well as single component fitting (M) and the corresponding fitting residuals (O), and bi-component fitting (N) and the corresponding fitting residuals (P). Free water residing in large pores (long thin arrow), periosteum (short thick arrow) and marrow fat residing in the inner and middle cortex (long thick arrow) are well depicted. An ROI was drawn in mid-cortex, avoiding free water, periosteum and marrow fat. Single component fitting shows significant residual signal (> 10%). The residual signal is reduced to less than 2% by bi-component fitting, which shows a shorter T2* of 0.34 ms and a longer T2* of 2.92 ms with respective fractions of 75.4% and 24.6% by volume.

There are no standard reference techniques available to accurately measure bound and free water in cortical bone. A bovine bone drying experiment was conducted to indirectly validate the results. **Figure 5** shows UTE images of bovine cortical bone before (A) and after (B) air-drying at room temperature for three days, as well as bi-component fitting (C) of UTE images of the wet bone. Figure 5C shows that there is a short T2 component (80.6%) and longer T2 component (19.4%) for wet bone. Free water is expected to very largely disappear after three days air-drying. Bi-component fitting indeed shows a near zero fraction of 0.7% for free water component, while bound water component accounts for 99.3% of the total UTE signal.

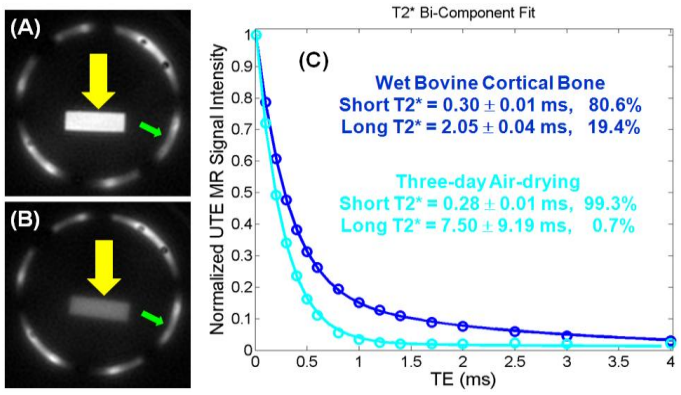

Fig 5 UTE imaging of a wet bone sample (long arrow) (A) and after 3-days air-drying (B). The surrounding coil is bright (short arrow). Free water fraction dropped from 19.4% for wet bone to 0.7% for dry-bone.

Figure 6 shows the correlation between UTE MR measured water loss and gravimetric bone

water loss of seven bovine cortical bone samples during sequential air-drying. There was a high correlation (R = 0.91; P < 0.0001) between UTE MR measured free water loss and gravimetric bone weight loss during sequential air-drying, and a significant correlation (R = 0.69; P < 0.01) between UTE bound water loss and gravimetric bone weight loss during oven-drying [55]. These results show that UTE bi-component analysis can be used to estimate bound and free water in cortical bone. The technique has potential applications for the in vivo evaluation of bone porosity and organic matrix.

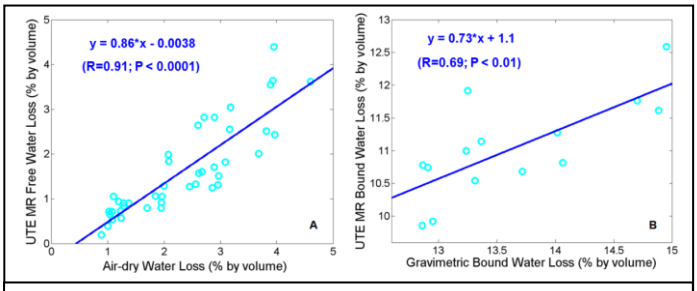

Fig 6 A high correlation was observed between UTE measured free water loss and gravimetric water loss during sequential air-drying (A), as well as UTE measured bound water loss and gravimetric water loss during oven-dry (B).

Selective Imaging of Bound Water in Cortical Bone Using IR-UTE Sequences

The bound water component can potentially be selectively imaged with both 2D IR-UTE and 3D IR-UTE sequences. In both cases relatively long single adiabatic inversion recovery (SIR) pulses (8.6 ms in duration) are employed to simultaneously invert the longitudinal magnetizations of long T2 water (including the free water component in cortical bone, muscle, etc) and fat (including bone marrow). The 2D and 3D UTE data acquisitions are then begun at an inversion time (TI) designed to allow the inverted free water and fat longitudinal magnetizations to closely approach the null point [43, 50, 59, 60].

We have developed techniques to image cortical bone with high spatial resolution and contrast, as shown in **Figure 7**. The IR-UTE sequence provides high contrast imaging of the ulna and radius as well as tendons of a forearm specimen in a total scan time of 9 min. Long T2 muscle and free water in cortical bone as well as marrow fat are believed to be well suppressed and water bound to the organic matrix is believed to contribute to the IR-UTE singal.

A single component T2* decay was observed in the single adiabatic inversion

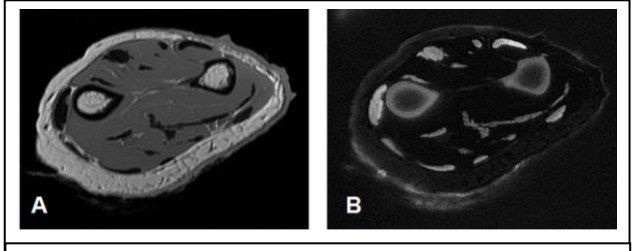

Fig 7 A cadaveric forearm imaged with a clinical 2D FSE sequence (A) and an SIR-UTE sequence (B). The 2D FSE sequence shows near zero signal for bone and tendon. These are depicted with high spatial resolution and contrast with the 2D SIR-UTE sequence.

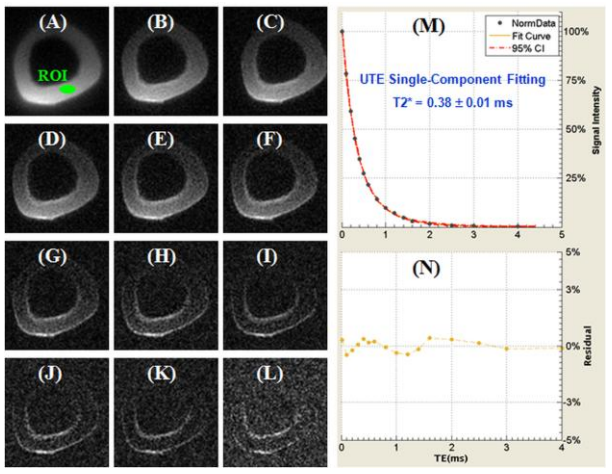

Fig 8 Selected non-slice selective 2D SIR-UTE imaging of the same human cortical bone sample shown in Figure 1 with TEs of 8 μs (A), 0.2 ms (B), 0.4 ms (C), 0.6 ms (D), 0.8 ms (E), 1.0 ms (F), 1.2 ms (G), 1.6 ms (H), 2.0 ms (I), 2.6 ms (J), 3.0 ms (K), and 4.0 ms (L), as well as single component fitting (M) and the corresponding fitting residuals (N). The residual signal is less than 0.5% by single component fitting, suggesting that only signal from bound water is detected with SIR-UTE imaging.

recovery (SIR) UTE images. **Figure 8** shows selected SIR-UTE images of the same cortical bone shown in Figure 15 as well as the corresponding single component curve fitting which accounted for 99.9% of the signal variance with the residual signal less than 0.5%. The fitted T2* of 0.38 ms was very close to the shorter T2* value of 0.34 ms from the bi-component fitting of UTE T2* signal decay. These results suggest that only one component, water bound to the organic matrix, exists in SIR-UTE imaging. The free water component with longer T2 was selectively suppressed by the SIR preparation pulse through adiabatic inversion and signal nulling.

Dual adiabatic inversion recovery (DIR) pulses can also be employed to invert and null signal from long T2 water and fat, respectively, followed by 2D or 3D UTE selective imaging of bound water in cortical bone. In this approach two long adiabatic inversion pulses are used to successively invert the longitudinal magnetization of long T2 water and long T2 fat [57]. The longitudinal magnetization of cortical bone with short T2 is not inverted due to significant transverse relaxation during the long adiabatic inversion process. The UTE acquisition starts at a delay time of TI1 necessary for the inverted long T2 water magnetization to reach the null point, and of TI2 for the inverted fat magnetization to also reach the null point. The long T2 water magnetization is inverted first (TI1 > TI2) because of its longer T1 and the fat magnetization is inverted later because of its shorter T1. Appropriate combination of TI1, TI2 and TR allows robust (insensitive to B_1 and B_0 inhomogeneities) and efficient simultaneous suppression of long T2 water and fat signals.

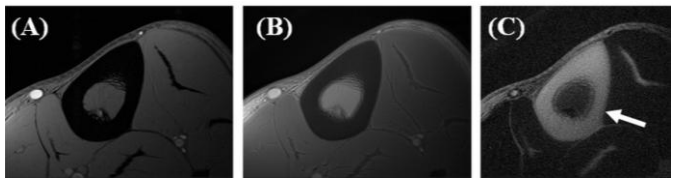

Fig 9 The mid-tibia of a volunteer imaged with the GRE (left), UTE (middle) and DIR-UTE (right) sequences. The GRE sequence shows a signal void for cortical bone. The regular UTE image shows slightly higher signal from bone but poor contrast. The DIR-UTE image selectively suppresses signal from fat and muscle, creating high contrast for cortical bone with an acquired voxel size of $0.2\times0.2\times5.0$ mm^3 in a total scan time of 5 minutes.

Figure 9 shows images of the left distal tibia of a 31 year old healthy male volunteer using clinical 2D gradient recalled echo (GRE), conventional UTE and DIR-UTE techniques with a FOV of 10 cm and a slice thickness of 5 mm. Two long adiabatic inversion pulses (duration ~ 25 ms, spectral bandwidth ~ 520 Hz) were centered at zero Hz (to cover the water peak and CH peak) and -440 Hz (to cover the CH_2 and CH_3 peaks), respectively, to provide effective coverage of the water and multiple fat peaks, allowing inversion of their longitudinal magnetization. A TI1 of 140 ms and TI2 of 110 ms were employed for long T2 suppression (TI2 is

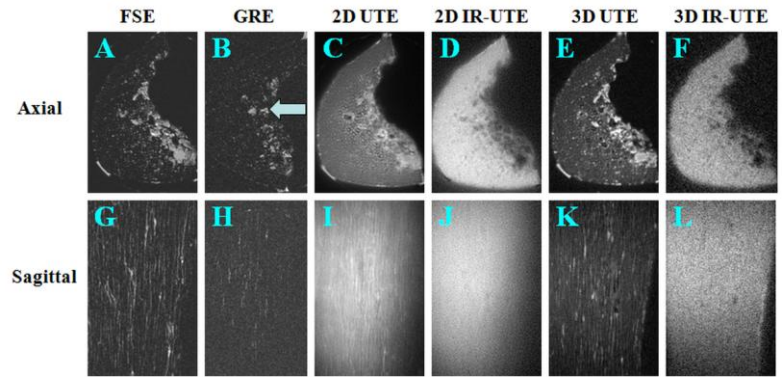

Fig 10 2D FSE (A, G), 2D GRE (B, H), 2D UTE (C, I), 2D SIR-UTE (D, J), 3D UTE (E, K) and 3D SIR-UTE (F, L) imaging of a cortical bone sample immersed in PFOB in the axial (1st row) and sagittal (2nd row) planes. Free water in the Haversian canals is detected by both FSE (A, G), 2D UTE (C, I) and 3D UTE (E, K) sequences. Both 2D SIR-UTE (D, J) and 3D SIR-UTE (F, L) show a uniform bright signal, consistent with only bound water being detected. GRE (B, H) shows little or no signal for both bound and free water in cortical bone. The bright signal shown in (B) corresponds to residual marrow fat (arrow).

suboptimal in order to avoid overlap between the two long adiabatic pulses). Cortical bone demonstrates a signal void with the 2D GRE sequence, and poor contrast with the conventional UTE sequence due to the high signal from the surrounding muscle and fat. The DIR-UTE sequence suppresses long T2 water signals (such as muscle and free water in bone) and fat, and displays cortical bone with high contrast and high signal from water bound to the organic matrix.

Figure 10 shows the results of 2D FSE, 2D GRE, 2D and 3D UTE, as well as 2D and 3D SIR-UTE imaging of a cortical bone sample [59]. Free water in the Haversian canals is well depicted by the 2D FSE sequence, but appears as a signal void with the 2D GRE sequence, consistent with free water having a long T2 but short T2* in cortical bone. The 2D and 3D UTE sequences detect both free water in the pores which appears as high signal fine structure, as well as water bound to the organic matrix which appears as uniform background signal. The high signal fine structure disappears with the 2D and 3D SIR-UTE sequence where the free water signal is suppressed by the adiabatic IR preparation pulse. The uniform background signal is probably from water bound to the organic matrix.

Quantitative Imaging of Bone Water Compartments

FSE imaging of cortical bone can potentially provide a quantitative measure of cortical porosity. Voxels with high signal intensity correspond to water residing in the macroscopic pores of cortical bone. A simple sum of all the voxels with signal intensity above a certain signal threshold is expected to provide an accurate measure of cortical porosity. We have compared FSE based cortical porosity with that from micro-CT imaging of nine human cortical bone samples. **Figure 11** shows selected 2D FSE imaging and μCT imaging of cortical bone samples. There is a high morphological correlation between these two imaging techniques, suggesting that 2D FSE imaging is able to detect cortical pore structure.

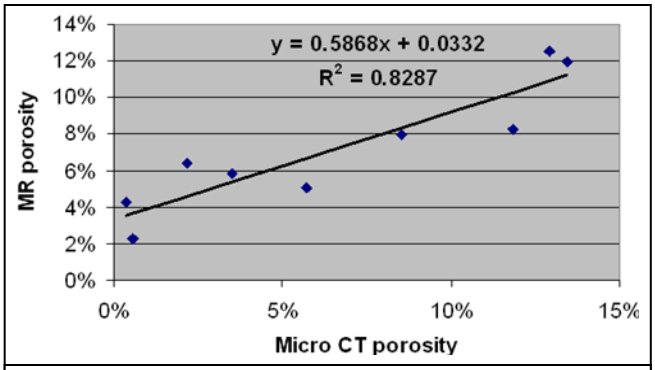

Fig 11 Correlation between FSE MRI and μCT porosity.

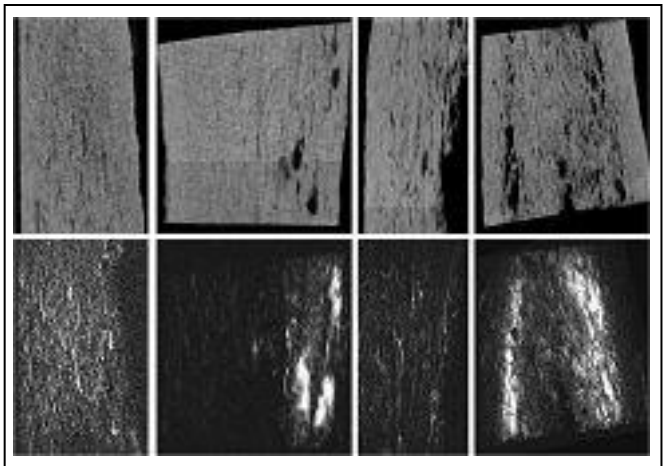

Fig 12 μCT (1st row) and FSE (2nd row) imaging of four human cortical bone samples. There is a high morphological correlation between these two imaging modalities.

Figure 12 shows the correlation between porosity assessed by μCT imaging and porosity assessed by 2D FSE MR imaging. There is a high correlation between these two imaging modalities ($R2 = 0.8287$; $P < 0.0001$), suggesting that clinical 2D FSE imaging can reliably assess cortical porosity.

UTE imaging of cortical bone can potentially provide a quantitative measure of total water, bound water and free water in cortical bone, which can be used to evaluate bone quality. **Figure 13** shows UTE, μCT

and mechanical testing of two bone samples. Bi-component analysis shows a long T2* fraction of 33% for #1 with a low porosity of 1.8%, and a long T2* fraction of 67% for #2 with a higher porosity of 6.8%. Sample #2 with the higher porosity had 38-55% lower failure strain, failure energy and ultimate stress.

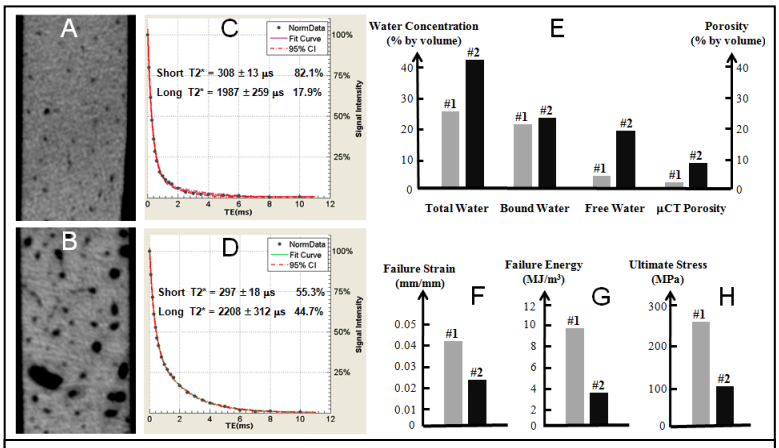

Fig 13 µCT shows a porosity of 1.7% for sample #1 (**A**) and 8.9% for sample #2 (**B**). UTE bi-component analyses (C, D) show 150% higher in long T2* fraction for sample #2 (44.7% vs. 17.9%), which has ~62% higher total water concentration and ~400% higher free water concentration (E), as well as ~55% lower failure strain (F), ~40% lower failure energy (G) and ~38% lower ultimate stress (H).

UTE images can also be used to measure absolute bone water by volume via comparison of signal from bone and that from a reference phantom. Total water concentration can be measured by comparing the UTE signal of cortical bone with that of the calibration phantom using standard Ernst equation. Bound water concentration can be measured by comparing SIR-UTE or DIR-UTE signal of bone with that of the calibration phantom. **Figure 14** shows conventional GRE, UTE and IR-UTE imaging of the tibia mid-shaft of a volunteer obtained with a quadrature knee coil. A total water content of 22.3% was found with UTE and a bound water content of 18.1% was found with IR-UTE, indicating a free water content of 3.5% by volume. A rubber eraser with similar T1 and T2*s was used as a calibration phantom for water content measurement.

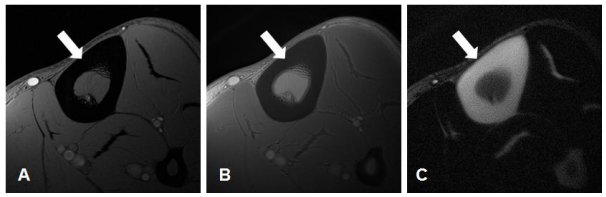

Fig 14 Axial imaging of the tibia mid-shaft in a volunteer using GRE (A), UTE (B) and IR- UTE (C) sequences. GRE shows zero signal for bone. UTE shows a total water content of 22.3%, while IR-UTE shows a bound water content of 18.1% by volume.

Figure 15 shows FSE, UTE and IR-UTE imaging of the tibia mid-shaft of volunteers with a 1-inch surface coil, which allows high resolution FSE images to be obtained with voxel sizes of 78×78×700 µm^3, with adequate SNR in a scan time of 6.5 minutes. High quality UTE and IR-UTE images are also achieved.

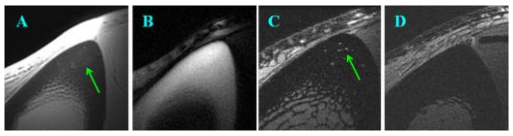

Fig 15 Axial imaging of the tibia mid-shaft of a 58- year old healthy volunteer with UTE (A), IR-UTE (B) and FSE (C) sequences, and FSE imaging of the tibia mid-shaft of a 39 year-old healthy volunteer (D). UTE detects signal from both bound and free water (A), while IR-UTE shows water bound to the organic matrix (B). Fine structures in FSE images correspond to the large Haversian canals (C). The younger volunteer shows no structure in cortical bone with the FSE sequence, consistent with bone without larger canals (D).

Conclusion

The bound and free water components in cortical bone show distinct T2* relaxation times but similar T1s. Both bone water components can be assessed with 2D and 3D UTE sequences. The bound water component can be selectively assessed with the IR-UTE or DIR-

UTE sequences, while the free water component can be selectively assessed with clinical 2D FSE sequences. Clinical GRE sequences provide little signal from cortical bone due to the short T2* of both bound and free bone water components.

Acknowledgement

The authors thank grants support from GE Healthcare, NIH and the Radiological Society of North America (RSNA) research and education foundation.

References

1. NIH consensus development panel on osteoporosis prevention, diagnosis, and therapy. JAMA 2001; 285:785-795
2. Schneider EL, Guralnik JM. The aging of America. Impact on health care costs. JAMA 1990; 263:2335-2340.
3. World Health Organization. Assessment of fracture risk and its application to screening for postmenopausal osteoporosis. WHO Technical Report Series 843. Geneva: WHO 1994.
4. Genant HK, Cooper C, Poor G, Reid I, Ehrlich G, Kanis J, Nordin BEC, Barrett-Connor E, Black D, Bonjour J-P, Dawson-Hughes B, Delmas PD, Dequeker J, Eis SR, Gennari Lindsay R, Martin TJ, Masri B, Mautalen CA, Meunier PJ, Miller PD, Mithal A, Morii H, Papapoulos S, Woolf A, Yu W, Khaltaev N. Interim report and recommendations of the World Health Organization task-force for osteoporosis. Osteoporos Int 1999; 10:295-264.
5. American Society for Bone and Mineral Research ASBMR Bone Curriculum 2004. http://depts.washington.edu/bonebio/ASBMRed/ASBMRed.html.
6. Zabaze RMD, Ghasem-Zadeh A, Bohte A, Luliano-Burns S, Mirams M, Price RI, Mackie EJ, Seeman E. Intracortical remodeling and porosity in the distal radius and post-mortem femurs of women: a cross-sectional study. Lancet 2010; 375:1729-1736.
7. Wehrli FW, Song HK, Saha PK, Wright AC. Quantitative MRI for the assessment of bone structure and function. NMR in Biomed 2006; 19:731-764.
8. Cowin SC. Bone poroelasticity. J Biomechanics 1999; 32:217-238.
9. Ritchie RO, Buehler MJ, Hansma P. Plasticity and toughness in bone. Physics Today 2009; June:41-47.
10. Cummings SR, Karpf DB, Harris F, Genant HK, Ensrud K, LaCroix AZ, Black DM. Improvement in spine bone density and reduction in risk of vertebral fractures during treatment with antiresorptive drugs. Am J Med 2002; 112:281-289.
11. De Lact C, van Hout B, Burger H, Hofman A, Pols H. Bone density and the risk of hip fracture in men and women: cross sectional analysis. Br Med J 1997; 315:221-225.
12. Brandi ML. Microarchitecture, the key to bone quality. Rheumatology 2009; 48:3-8.
13. Cummings SR, Nevitt MC, Browner WS, Stone K, Fox KM, Ensrud KE, Cauley J, Black D, Vogt TM. Risk factors for hip fracture in white women. Study of osteoporotic fractures research group. N Engl J Med 1995; 332:767-773.
14. Miller PD, Bonnick SL, Rosen CJ, Altman RD, Avioli LV, Dequeker J, Felsenberg D, Genant HK, Gennari C, Harper KD, Hodsman AB, Kleerekoper M, Mautalen CA, McClung MR, Meunier PJ, Nelson DA, Peel NF, Raisz LG, Recker RR, Utian WH, Wasnich RD, Watts NB, Clinical utility of bone mass measurements in adults: consensus of an international panel. Semin Arthritis Rheum 1996; 25:361-372.
15. Thompson DD. Age changes in bone mineralization: cortical thickness and Haversian canal area. Calcif Tissue Int 1980; 31:5-11.
16. McCalden RW, McGeough JA, Barker MB, Court-Brown CM. Age-related changes in the tensile properties of cortical bone: the relative importance of changes in porosity, mineralization and microstructure. J Bone Joint Surg Am 1993; 75:1193-1205.
17. Diab T, Vashishth D. Effects of damage morphology on cortical bone fragility. Bone 2005; 37:96-102.
18. Martin RB, Burr DB. The microscopic structure of bone. In: Structure, function, and adaptation of compact bone. New York, NY, USA: Raven Press, 1989.
19. Bousson V, Meunier A, Bergot C, Vicaut E, Rocha MA, Morais MH, Laval-Jeantet AM, Laredo JD. Distribution of intracortical porosity in human midfemoral cortex by age and gender. J Bone Miner Res 2001; 16:1308-1317.
20. Schaffler MB, Burr DB. Stiffness of compact bone: effects of porosity and density. J Biomech 1988; 21:13-16.
21. Currey J. The effect of porosity and mineral content on Young's modulus of elasticity of compact bone. J Biomech 1988; 21:131-139.
22. Yeni YN, Brown CU, Norman TL. Influence of bone composition and apparent density on fracture toughness of the human femur and tibia. Bone 1998; 22:79-84.

23. Epstein S. Is cortical bone hip? What determines cortical bone properties? Bone 2007; 41:S3-S8.
24. Jordan GR, Loveridge N, Bell KL, Power J, Rushton N, Reeve J. Spatial clustering ofremodeling osteons in the femoral neck cortex: a cause of weakness in hip fracture? Bone 2000; 26:305-313.
25. Wall J, Chatterji S, Jeffery J. Age-related changes in the density and tensile strength of human femoral cortical bone. Calcif Tiss Int 1979; 27:105-108.
26. Nishiyama KK, Macdonald HM, Buie HR, Hanley DA, Boyd SK. Postmenopausal women with osteopenia have higher cortical porosity and thinner cortices at the distal radius and tibia than women with normal aBMD: an in vivo HR-pQCT study. J Bone Miner Res 2010; 25:882-890.
27. Burghardt AJ, Kazakia GJ, Ramachandran S, Link TM, Majumdar S. Age and gender related differences in the geometric properties and biomechanical significance of intra-cortical porosity in the distal radius and tibia. J Bone Miner Res 2009;
28. Martin RB, Ishida J. The relative effects of collagen fiber orientation, porosity, density, and mineralization on bone strength. J Biomech 1989; 22:419-426.
29. Boskey AL, Wright TM, Blank RD. Collagen and bone strength. J Bone Miner Res 1999; 14:330-335.
30. Zioupos P, Currey JD, Hamer AJ. The role of collagen in the declining mechanical properties of aging human cortical bone. J Biomed Mater Res 1999; 45:108-116.
31. Lees S. A mixed pacing model for bone collagen. Calcif Tissue Int 1981; 33:591-602.
32. Wang X, Shen X, Li X, Mauli Agrawal C. Age-related changes in the collagen network and toughness of bone. Bone 2002; 31:1-7.
33. Neuman WF, Neuman MW. Skeletal dynamics the chemical dynamics of bone mineral. Chicago: Univ of Chicago Press 1958, pp.101.
34. Robinson RA, Elliot SR. The water content of bone. J Bone Joint Surg 1957; 39:167-188.
35. Elliott SR, Robinson RA. The water content of bone. I. The mass of water, inorganic crystals, organic matrix, and CO2 space components in a unit volume of the dog bone. J Bone Joint Surg Am 1957; 39(A):167–188.
36. Timmins PA, Wall JC. Bone water. Calcif Tissue Res 1977; 23:1-5.
37. Mueller KH, Trias A, Ray RD. Bone density and composition: age-related and pathological changes in water and mineral content. J Bone Joint Surg Am 1966;48:140 –148.
38. Morris MA. Lopez-Curto JA, Hughes SPF, An K, Bassingthwaighte JB, Kelly PJ. Fluid spaces in canine bone and marrow. Microvascular research.1982; 32:188-200.
39. Cowin SC. Bone poroelasticity. J Biomechanics 1999; 32:217-238.
40. Horch RA, Gochberg DF, Nyman JS, Does MD. Non-invasive Predictors of Human Cortical Bone Mechanical Properties: T-2-Discriminated H-1 NMR Compared with High Resolution X-ray. PLoS ONE 2011;6(1):e16359.
41. Nyman JS, Ni Q, Nicolella DP, Wang X. Measurements of mobile and bound water by nuclear magnetic resonance correlate with mechanical properties of bone. Bone 2008; 42:193-199.
42. Horch RA, Nyman JS, Gochberg DF, Dortch RD, Does MD. Characterization of 1H NMR signal in human cortical bone for magnetization resonance imaging. Magn Reson Med 2010; 64:680-687.
43. Horch R, Gochberg D, Nyman J, Does M. Clinically-compatible MRI strategies for discriminating bound and pore water in cortical bone. Magn Reson Med 2012 (Epub Jan 31).
44. Ong HH, Wright AC, Wehrli F. Deuterium nuclear magnetic resonance unambiguously quantifies pore and collagen-bound water in cortical bone. J Bone Miner Res 2012; in press.
45. Wu Y, Ackerman JL, Chesler DA, Graham L, Wang Y, Glimcher MJ. Density of organic matrix of native mineralized bone measured by water- and fat-suppressed proton projection MRI. Magn Reson Med 2003; 50:59-68.
46. Cao H, Ackerman JL, Hrovat MI, Graham L, Glimcher MJ, Wu Y. Quantitative bone matrix density measurement by water- and fat-suppressed proton projection MRI (WASPI) with polymer calibration phantoms. Magn Reson Med 2008; 60:1433-1443.
47. Cao H, Nazarian A, Ackerman JL, Snyder BD, Rosenberg AE, Nazarian RM, Hrovat MI, Dai G, Mintzopoulos D, Wu Y. Quantitative 31P NMR spectroscopy and 1H MRI measurements of bone mineral and matrix density differentiate metabolic bone diseases in rat models. Bone 2010; 46:1582-1590.
48. Techawiboonwong A, Song HK, Wehrli FW. In vivo MRI of submillisecond T2 species with two-dimensional and three-dimensional radial sequences and applications to the measurement of cortical bone water. NMR in Biomed 2008; 21:59-70.
49. Techawiboonwong A, Song HK, Leonard MB, Wehrli FW. Cortial bone water: in vivo quantification with ultrashort echo-time MR imaging. Radiology 2008; 248:824-833.
50. Du J, Carl M, Bydder M, Takahashi A, Chung CB, Bydder GM. Qualitative and quantitative ultrashort echo time (UTE) imaging of cortical bone. J Magn Reson 2010; 207:304-311.

51. Reichert ILH, Robson MD, Gatehouse PD, He T, Chappell KE, Holmes J, Girgis S, Bydder GM. Magnetic resonance imaging of cortical bone with ultrashort TE (UTE) pulse sequences. Magn Reson Imaging 2005; 23:611-618.
52. Du J, Hamilton G, Takahashi A, Bydder M, Chung CB. Ultrashort TE spectroscopic imaging (UTESI) of cortical bone. Magn. Reson. Med. 2007; 5:1001-1009.
53. Kokabi N, Bae W, Diaz E, Chung CB, Bydder GM, Du J. Ultrashort TE (UTE) MR imaging of bovine cortical bone: the effect of water loss on the T1 and T2* relaxation times. Magn Reson Med 2011; 66:476-482.
54. Du J, Diaz E, Carl M, Bae WC, Chung CB, Bydder GM. Ultrashort echo time imaging with bicomponent analysis. Magn Reson Med 2012; 67:645-649.
55. Biswas R, Bae CW, Diaz E, Masuda K, Chung CB, Bydder GM, Du J. Ultrashort echo time (UTE) imaging with bi-component analysis: bound and free water evaluation of bovine cortical bone subject to sequential drying. Bone 2012; 50:749-755.
56. Bae WC, Chen PC, Chung CB, Masuda K, DLima D, Du J. Quantitative ultrashort echo time (UTE) MRI of human cortical bone: correlation with porosity and biomechanical properties. J Bone Miner Res 2012; 27:848-857.
57. Du J, Takahashi A, Bae WC, Chung CB, Bydder GM. Dual inversion recovery, ultrashort echo time (DIR UTE) imaging: creating high contrast for short-T2 species. Magn Reson Med 2010; 63:447-455.
58. Du J, Bydder M, Takahashi AM, M Carl, Chung CB, Bydder GM. Short T2 contrast with three-dimensional ultrashort echo time imaging. Magn Reson Imaging 2011; 29:470-82.
59. Du J, Hermida JC, Diaz E, Corbeil J, Znamirowski R, D'Lima DD, Bydder GM. Assessment of cortical bone with clinical and ultrashort echo time sequences. Magn Reson Med 2012 Sep 21 [Epub ahead of print].
60. Du J, Bydder GM. Qualitative and quantitative ultrashort-TE MRI of cortical bone. NMR Biomed 2012 Dec 28 [Epub ahead of print].
61. Bell KL, Loveridge N, Power J, Garrahan N, Meggitt BF, Reeve J. Regional differences in cortical porosity in the fractured femoral neck. Bone 1999; 24:57-64.